Optics Letters

# Bound state of asymmetric pure-quartic solitons in motion

Chunxiang Zhang,[1] Zhixiang Deng,[2] Rui Ma,[2] Haiyang Lu,[1] Dianyuan Fan,[2] and Jun Liu[2,*]

[1]Shenzhen Key Laboratory of Ultraintense Laser and Advanced Material Technology, Center for Advanced Material Diagnostic Technology, College of Engineering Physics, Shenzhen Technology University, Shenzhen 518118, China
[2]International Collaborative Laboratory of 2D Materials for Optoelectronics Science & Technology, Institute of Microscale Optoelectronics, Shenzhen University, Shenzhen 518060, China
*liu-jun-1987@live.cn

Received 25 September 2024; revised 7 November 2024; accepted 7 November 2024; posted 11 November 2024; published 10 December 2024

**In this Letter, we investigate the binding mechanism and motion dynamics of the bound state consisting of two pure-quartic solitons (PQSs) with unequal intensities and find that their movement occurs as an entity under the Raman self-frequency shift. By calculating the forces that induce the relative motion between the unequal PQSs, we derive the balanced conditions for maintaining a near-constant separation and the constant phase profile between them. The predictions are validated by the numerical simulations. Our work provides insights into the intrinsic features of symmetry-broken localized structures in nonlinear–dispersive systems, stimulating interest in asymmetric multi-soliton states with intriguing dynamics.** 

https://doi.org/10.1364/OL.542762

The solitons are shape-preserving localized structures owing to the self-organization in nonlinear systems that have been studied in various fields, such as nonlinear optics [1,2] and hydrodynamics [3,4]. In nonlinear optics, the conventional solitons arise from a delicate balance between the nonlinearity and the second-order dispersion (SOD), the temporal profiles of which are featuring a hyperbolic-secant shape. The solitary pulse shape and its other propagating characteristics can be manipulated through the combined dispersive and nonlinear effects [1]. Recently, a new class of solitons, termed as pure-quartic solitons (PQSs), was experimentally observed from typical dispersion engineered mode-locked fiber lasers incorporating a spectral pulse shaper [5–7]. They are generally formed under the condition that the fourth-order dispersion (FOD) dominates over other-order dispersions [8–11]. This particular class of solitons can possess a unique energy-width scaling relation, which is promising for designing high-energy soliton lasers [5]. The temporal profiles of PQSs include a main Gaussian pulse part and two oscillating tails with low amplitude at the both side edges [8]. The overlapping of tails can induce weak interactions between two well-separated PQSs, establishing the effective trapping and assembling into a robust structure [12–15]. This type of double-humped structure is also called a bound state (BS) of PQSs [16,17], exhibiting stable evolution without distortion and featuring discrete separations.

Up to now, the works on the BS of PQSs mainly concentrate on the symmetric cases with an equal intensity, while the asymmetric BS of PQSs composed of unequal solitons are rarely discussed. However, the research on the latter configuration can be beneficial to the understanding of nonlinear interactions among them and the symmetry breaking in conservation systems. Compared with the symmetric case, the superposition of unequal paired PQSs cannot satisfy the condition of stationary $\exp(i\mu z)$ dependence ($\mu > 0$ is the propagation constant) and thus do not have a uniform phase over their profiles, allowing for an energy flow process within the double-hump structure [10,11]. Besides the common intrinsic parameters (e.g., the separation and relative phase) used to characterize the symmetric BSs [18,19], the asymmetric case also includes additional degrees of freedom, such as the parameter reflecting the exact asymmetric structure. These important features can be identified to describe the asymmetric multi-PQS patterns with interesting features. Moreover, in contrast to the traditional solitons, the PQSs can bear intrinsic advantages of supporting much higher peak power and energies as well as a broader spectrum [8–11]. Therefore, the stimulated Raman scattering (SRS) [1,20] tends to occur during the PQS generation and evolution in nonlinear mediums. In this sense, the Raman-perturbed interaction dynamics between the unequal PQSs are very important and worth to be investigated.

Here, we numerically and analytically unveil the evolutionary behaviors of the asymmetric BSs constituted by two unequal PQSs with overlapping tails. The forces involving the Kerr-mediated interaction and the Raman self-frequency shift are calculated based on a modified perturbation model. Then, we derive the balanced conditions for the equal-acceleration and constant phase constraint which can support the stable motion of paired PQSs under the Raman self-frequency shift. Numerical simulations are performed to validate the analytical predictions.

In the regime of the vanishing SOD and dominant FOD, the evolution of a pulse envelope $A(z, t)$ can be well described by the generalized nonlinear Schrödinger equation (NLSE) [8] with a linearized form of the Raman term [1] (response time of $T_R$),

which can be written as follows:

$$\frac{\partial A}{\partial z} = \frac{i}{24}\beta_4 \frac{\partial^4 A}{\partial t^4} + i\gamma|A|^2 A - i\gamma T_R A \frac{\partial |A|^2}{\partial t}, \tag{1}$$

where $z$ is the distance, $t$ is the retarded time, and $\beta_4$, $\gamma$ represent the parameters of FOD and nonlinearity, respectively. To investigate the underlying evolutionary dynamics of the asymmetric PQS BS, the input optical field is a linear superposition of a pair of well-separated PQSs, i.e., $A = U + V \cdot e^{i\varphi}$. Here, $U\,(V)$ is the leading (trailing) PQS envelope that is forwarded (trailed) in time by $\sigma/2$ (with a separation $\sigma$). The profiles of PQSs, obtained numerically using the Newton conjugate-gradient algorithm [21], are solely determined by the parameter $\mu$ when the parameters $\beta_4$, $\gamma$ are fixed. Here, $\varphi$ is the initial relative phase within the PQS pair and only takes two cases: 0 or $\pi$, i.e., in-phase or anti-phase, which can simplify the pulse interaction situations. To characterize the asymmetric properties of BSs, we introduce a variable $r$ denoting the peak power ratio between the leading pulse and the trailing one (i.e., $|U|^2 = r|V|^2$). Since the PQS parameter $\mu$ is proportional to its peak power [8], the variable $r$ is equivalent to the ratio of their $\mu$ values.

In this configuration, we introduce the particle-like model where the PQS pulses propagate as stable entities. An optical "bond" connecting two PQSs (analogy with atoms) is a common zone formed by their overlapping tails, which can act as a perturbed role. Therefore, considering the perturbative approach in [22–24], the Kerr-mediated interaction forces induced by the overlapping tails and the Raman force, respectively, can be written as follows:

$$\frac{d}{dz}\langle f\rangle_{U,V} = -\gamma \frac{\int P_{U,V}(t)\frac{\partial(|U+Ve^{i\varphi}|^2)}{2\pi\,\partial t}\mathrm{d}t}{\int P_{U,V}(t)\mathrm{d}t}, \quad \frac{d}{dz}\Omega_{R,U,V} = -\gamma T_R \frac{\int P_{U,V}(t)\frac{\partial^2 P_{U,V}(t)}{2\pi\,\partial t^2}\mathrm{d}t}{\int P_{U,V}(t)\mathrm{d}t}. \tag{2}$$

The details and arguments concerning Eq. (2) are presented in the Supplement 1. Here $P_{U(V)}(t) = |U|^2(|V|^2)$. Obviously, the former interaction force applies to both of the mutual pulses, which is related to the temporal separations between $U$ and $V$. Instead, the latter one acts on the individual pulses regardless of their exact separations. Therefore, the net force acting on each pulse in motion is as follows:

$$\frac{d}{dz}\Omega_{U,V} = \frac{d}{dz}\langle f\rangle_{U,V} + \frac{d}{dz}\Omega_{R,U,V}. \tag{3}$$

The above formulas reflect the frequency offsets for the centroid of each PQS pulse. Figure 1 shows the amplitude envelopes and effective forces for the superposition of two well-separated PQSs with in-phase or anti-phase. Figures 1(a) and 1(c) show the amplitude envelopes of the PQS pair: $U$ is indicated by a blue line, while $V$ is represented by a brick-red line; the profiles for the superposition of two unequal pulses ($U$ and $V$) are filled by shadows with color. Figures 1(b) and 1(d) show the net force acting on $U$ and $V$ as a function of their separation $\sigma$ for the anti- and in-phase cases, respectively. Their respective net forces, as displayed by distinct colored lines, are not symmetric owing to two PQSs with unequal intensities. The intersection points marked by the black circles filled with red dots indicate the balancing forces, which are a prerequisite for the formation of asymmetric BSs. In contrast a traditional soliton [24], the balancing point is not unique, as shown in Figs. 1(b) and 1(d).

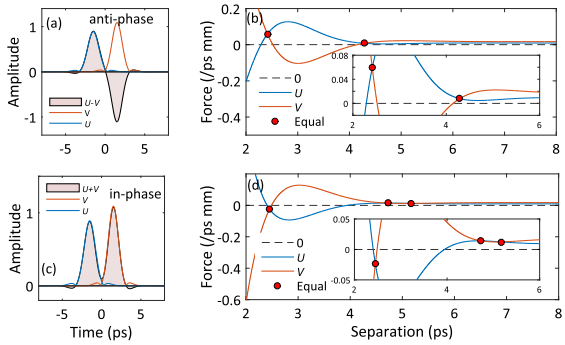


**Fig. 1.** Forces acting on the asymmetric PQS pair with the ratio $r = 0.7$, including the anti-phase (upper row) and in-phase (below row) cases. First column: amplitude profiles of both pulses, at a certain separation, along with their corresponding superposition (filled by brick-red). Second column: the net results from both the Kerr-mediated interaction force and the Raman one. The equal of the respective net forces occurs at the intersection marked by some red dots with black circles. Parameters: $\beta_4 = -2.2\ \mathrm{ps}^4\ \mathrm{mm}^{-1}$, $\gamma = 4.072\ \mathrm{W}^{-1}\ \mathrm{mm}^{-1}$, $T_R = 2$ fs; the parameter $\mu$ of the leading pulse $U$ is $3\ \mathrm{mm}^{-1}$.

The equilibrium states for the asymmetric PQS BSs occur under the balancing condition for the forces. It's called an *equal-acceleration constraint* and can be written as follows:

$$\frac{d}{dz}\Omega_U = \frac{d}{dz}\Omega_V. \tag{4}$$

The two PQSs are equally accelerated as an entity, when satisfying Eq. (4), maintaining constant separation during the evolutions (at least in the initial stage). Based on the numerical simulations of Eq. (1) with a reliable split-step Fourier method [25], the specific examples on equal-acceleration constraints are presented in Figs. 2(a) and 2(b) for the anti-phase and in-phase superposition of two unequal PQSs, respectively, with the initial separations of 2.415 ps and 2.449 ps that correspond to the first intersection points of Figs. 1(b) and 1(d). Obviously, the weak interaction between them contributes to the stationary evolution over a distance of 1 mm (≈18 dispersion lengths), confirming that the BSs constructed by two unequal PQSs can propagate stably.

In the presence of the dispersive effect, the net frequency shift at the equilibrium can reflect, with relative to the reference frame, the velocity of an asymmetric BS of PQS behaving as a robust unit. From the first intersection of the insets in Figs. 1(b) and 1(d), the net frequency shift for the anti-phase case is positive, while it is negative for the in-phase case. As a result of the negative FOD, the BS entity in the former case runs slower, while the latter one behaves faster. To this end, Fig. 2(c) displays the time-shifted motion process for the centroid of the temporal profiles ($t_c = \int t|A|^2 dt / \int |A|^2 dt$), which is extracted from Figs. 2(a) and 2(b) (the evolution results of their relative phases are presented in Supplement 1). These are in sharp contrast to the separate Raman-induced deceleration of the individual pulse [1,20]. These results also show that the Raman-induced repulsion that leads to an increasing separation between two dissimilar PQSs can be counterbalanced by the Kerr-mediated attraction.

Furthermore, we also aim to investigate the global characteristics of the asymmetric PQS BSs through varying the asymmetry parameter $r$. Based on the perturbation theory above, within the

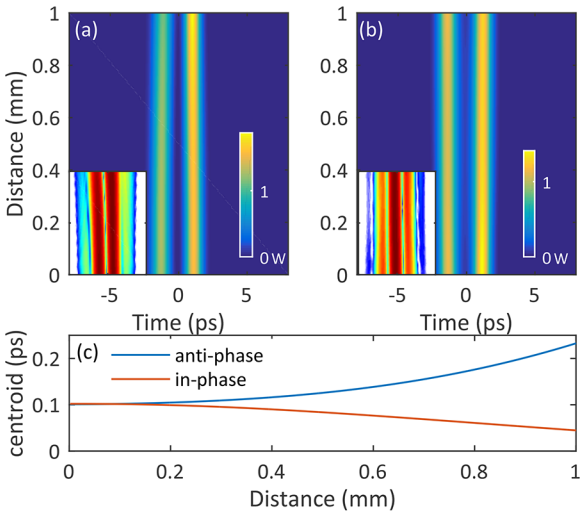


**Fig. 2.** Typical dynamics of the asymmetric PQS pair at the positions where the net forces acting on $U$ and $V$ are equal, marked by the red dots with black circles in Figs. 1(b) and 1(d). Upper row: the power profiles of anti-phase (a) and in-phase (b) PQS pairs evolving across a 1 mm distance (≈18 dispersion lengths) and their corresponding spectral evolutions are shown in the inserts at the bottom-left. (c) The evolutions of centroid of the temporal profiles for both the anti- and in-phase cases, illustrating the decelerating/accelerating motions of the asymmetric PQS BS, respectively.

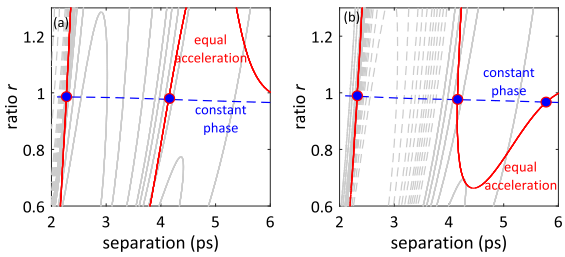


**Fig. 3.** Balancing conditions for the asymmetric BS of PQSs. The forces acting on the leading pulse $U$ are represented by gray contour curves, the solid curves of which represent the repulsion, while the dashed ones indicate the attraction. The points where the equal-acceleration and constant phase constraints are satisfied are connected by the red solid and blue dashed lines, respectively. The parameters are the same as in Fig. 1.

$(r, \sigma)$ parameter plane, the point trajectories satisfying the equal-acceleration constraint (Eq. (4)) are shown by the red solid curve in Fig. 3. Figure 3(a) represents the superposition of two PQSs with anti-phase, while Fig. 3(b) corresponds to the in-phase case. Besides, the force $(d\Omega_U/dz)$ acting on the leading soliton $U$ is also showed by the gray lines, indicating the direction of motion for the stationary BSs. The positive value marked by the gray solid line indicates that the BS becomes slower as a stable entity, while the gray dashed line corresponds to the opposite situation. Obviously, the equal-acceleration constraint does not require $r < 1$, which is different for the case of traditional solitons [24]. For both the in-phase and anti-phase cases, the separation range can be divided into two distinct parts: the region from 2 ps to 3 ps and the other one from 3 ps to 6 ps, which correspond to the strongly and loosely bounded states, respectively.

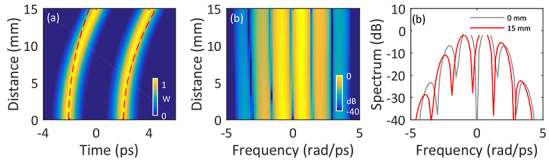


**Fig. 4.** Evolution of the asymmetric BS of PQSs that fulfills both the equal-acceleration and constant phase constraints. Both pulses are out of phase and the selected $(r, \sigma)$ correspond to the second intersection between the red curves and the blue ones in Fig. 3(a). (a) Temporal evolution; (b) spectral evolution; (c) spectral profiles at $z = 0$ and 15 mm. Red dashed curves in (a) mark the trajectories of the individual PQSs assuming the absence of the other PQS.

For the evolutions of asymmetric PQS pairs in Fig. 2, the energy flow among them can continue as a result of the rotating relative phase [23] induced by their distinct $\mu$ values, and they finally collide or break up. Therefore, in the strict manner, the preserved profiles of these doubly hump structures also need to satisfy the *constant phase constraint* [24]. This requirement is much more demanding, and thus the parameter range capable of supporting the asymmetric BSs is further narrowed down. The phase shifts involve two aspects: one is the phase offset induced by the distinct propagation constants $\mu$, and the other is a linear phase tilt caused by the net frequency shift of the PQS pair as an object. This constraint can be satisfied only when the relative phase in the middle time $(t_c)$ between the two PQSs is a constant. So, the expression can be written as follows:

$$\frac{d}{dz}\Delta\varphi(t_c) = \mu_V(1-r) - \frac{\sigma}{2}\frac{d}{dz}(\Omega_U + \Omega_V) = 0. \tag{5}$$

The trajectory of the point $(r, \sigma)$ satisfying the condition Eq. (5) is presented by the blue dashed line in Fig. 3. Its intersections with the equal-acceleration constraint are not unique and appear in both strongly and weakly bound intervals. These points can be termed as the *magic points* [24] and allow for maintaining both the intensity and the phase profiles of the PQS pair.

To confirm the characteristics of the equilibrium solution at the magic point mentioned above, we numerically calculate the evolutionary behavior of the asymmetric BS of PQSs over a long distance (15 mm, around 280 dispersion lengths). The initial parameters are taken as $\sigma = 4.1592$ ps and $r = 0.975$, which correspond to the intersection point in the loosely BS region. In this case, the magic point reflects the less obviously asymmetric features in terms of the small intensity differences between the two PQSs. However, the treatment can still be useful in the design of generating obviously asymmetric PQS BS. In Fig. 4(a), the whole structure deceleration is plainly visible but without obvious change in the shape of the pulse pair. For comparison, the dynamic trajectories of each soliton are also provided by the red dashed curves in Fig. 4(a) under the absence of the other soliton. Accordingly, in Figs. 4(b) and 4(c), the spectrum undergoes a global shift, which is indicative of the constant phase soliton pair. This is different from the insets in Figs. 2(a) and 2(b), where the visible spectral fringes represent a rotation of the relative phase. These results indicate that the evolution pertaining to the magic points satisfies the two constraints simultaneously. Note that such a quasi-invariant structure cannot be maintained infinitely. This can be explained as follows: the intensities of the Raman-decelerated PQSs are significantly reduced owing to the loss of energy entering into the radiation, which further induces the

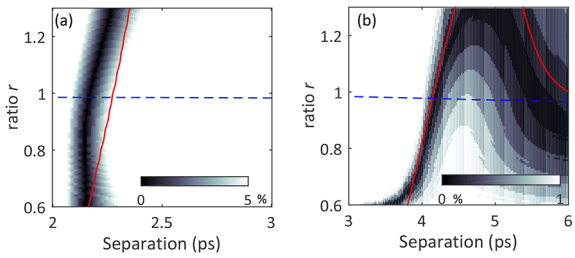


**Fig. 5.** Numerical results for the percentage of absolute value for the deviation between the FWHE of the double-humped structures at the input and at the output after a certain distance. The PQS pairs propagating along an equal-acceleration curve (predicted by the red solid curve) have nearly a constant separation when varying the initial ratio and separation. (a) and (b) represent the strongly and loosely bounded regions. The red and blue dashed lines are the same as those in Fig. 3(a).

rapid phase evolution and thus weakens the interaction between adjacent PQSs [23].

To compare with the results predicted in Fig. 3, both the ratios $r$ and separations $\sigma$ are varied to systematically investigate the evolution behaviors of the asymmetric BSs. We discuss separately the cases of the strongly and loosely bounded states. The preferred metric for the separation of the PQS pair is the full width at half-energy (FWHE) of the double-humped structure. The freeze of this value implies the stable propagation. Thus, we need to focus on the deviations. For each point on the ($r$, $\sigma$) plane, the absolute values of the maximum difference between the two FWHEs at the input and any later positions are presented in Fig. 5 for the anti-phase case. Figure 5(a) corresponds to a tight binding separation between 2 ps and3 ps, after a 1 mm propagation distance, and the results of the loosely bounded region in between 3 ps and 5 ps at 2 mm propagation distance are illustrated in Fig. 5(b). In each case they can be obtained from $2\times10^4$ simulation runs. Obviously, the constant separations can well reproduce the equal-acceleration prediction in Fig. 3(a). The deviation between the simulation results and the predicted ones is minimal quantitatively. Also, the numerical results demonstrate the existence of a class of metastable asymmetric PQS BSs, even when the $r$ value deviates from unity markedly or from the magic points mentioned above. The in-phase situation can also recreate the prediction in Fig. 3(b), which will not be shown here.

In conclusion, we derive the conditions for the equilibrium solution of the asymmetric BS of PQSs based on the analytical model of perturbation. The binding mechanism of the asymmetric PQS BSs and their interesting dynamics can be attributed to the periodic oscillations in the exponentially decaying tails of the temporal profiles. Different from the similar configuration with traditional solitons [24], the stationary configuration of PQS BSs does not require $r<1$, and the solutions satisfying the two constraints (i.e., the equal-acceleration and the constant phase) are not unique. We present numerical simulations by comparison with its predictions.

**Funding.** National Natural Science Foundation of China (12304478); Guangdong Basic and Applied Basic Research Foundation (2024A1515012152, 2022A1515010326); Guangdong Province Key Construction Discipline Scientific Research Capacity Improvement Project (2021ZDJS107); Science and Technology Planning Project of Shenzhen Municipality (JCYJ20220818100019040, JCYJ20230808105713028).

**Disclosures.** The authors declare no conflicts of interest.

**Data availability.** Data underlying the results presented in this Letter are not publicly available at this time but may be obtained from the authors upon reasonable request.

**Supplemental document.** See Supplement 1 for supporting content.

## REFERENCES

1. G. P. Agrawal, *Nonlinear Fiber Optics*, 4th ed. (Academic Press, 2007).
2. Y. S. Kivshar and G. P. Agrawal, *Optical Solitons: from Fibers to Photonic Crystals* (Academic Press, 2003).
3. D. H. Peregrine, J. Aust. Math. Soc. Series B, Appl. Math **25**, 16 (1983).
4. R. Camassa and D. D. Holm, Phys. Rev. Lett. **71**, 1661 (1993).
5. A. Runge, D. Hudson, K. Tam, *et al.*, Nat. Photonics **14**, 492 (2020).
6. J. Lourdesamy, A. Runge, T. Alexander, *et al.*, Nat. Phys. **18**, 59 (2022).
7. A. Runge, Y. Qiang, T. Alexander, *et al.*, Phys. Rev. Res. **3**, 013166 (2021).
8. K. Tam, T. Alexander, A. Redondo, *et al.*, Opt. Lett. **44**, 3306 (2019).
9. C. de Sterke, A. Runge, D. Hudson, *et al.*, APL Photonics **6**, 091101 (2021).
10. J. Widjaja, E. Kobakhidze, T. Cartwright, *et al.*, Phys. Rev. A **104**, 043526 (2021).
11. C. de Sterke and A. Blanco-Redondo, Opt. Commun. **541**, 129560 (2023).
12. A. V. Buryak and N. N. Akhmediev, Phys. Rev. E **51**, 3572 (1995).
13. D. Turaev, A. G. Vladimirov, and S. Zelik, Phys. Rev. Lett. **108**, 263906 (2012).
14. V. Afanasjev, B. Malomed, and P. Chu, Phys. Rev. E **56**, 6020 (1997).
15. M. Stratmann, T. Pagel, and F. Mitschke, Phys. Rev. Lett. **95**, 143902 (2005).
16. J. Zeng, J. Dai, W. Hu, *et al.*, Appl. Math. Lett. **129**, 107923 (2022).
17. J. Dai, J. Zeng, W. Hu, *et al.*, Chaos, Solitons Fractals **165**, 112867 (2022).
18. B. A. Malomed, Phys. Rev. A **44**, 6954 (1991).
19. A. G. Vladimirov, G. V. Khodova, and N. N. Rosanov, Phys. Rev. E **63**, 056607 (2001).
20. F. Mitschke and L. Mollenauer, Opt. Lett. **11**, 659 (1986).
21. J. Yang, J. Comput. Phys. **228**, 7007 (2009).
22. A. Hause, H. Hartwig, M. Böhm, *et al.*, Phys. Rev. A **78**, 063817 (2008).
23. A. Hause and F. Mitschke, Phys. Rev. A **80**, 063824 (2009).
24. A. Hause, T. Tran, F. Biancalana, *et al.*, Opt. Lett. **35**, 2167 (2010).
25. R. Deiterding, R. Glowinski, H. Oliver, *et al.*, J. Lightwave Technol. **31**, 2008 (2013).